Green synthesis of ZnO nanoparticles from citrus hystrix extracts for antibacterial application

M. A. Al-Wafiy Lauthfi [a], M. Z. M. Yusoff [a,b,c*], S. A. Kamil [a,b],
S. A. S. Mohamad [d], C. A. C. Abdullah [e], N. U. Saidin [f]

[a] *School of Physics and Material Studies, Faculty of Applied Sciences, Universiti Teknologi MARA, 40450 Shah Alam, Malaysia*
[b] *NANO-SciTech Lab (NST), Centre for Functional Materials and Nanotechnology (CFMN), Institute of Sciences (IOS), Universiti Teknologi MARA, 40450 Shah Alam, Malaysia*
[c] *Institute for Biodiversity and Sustainable Development (IBSD), Universiti Teknologi MARA, 40450 Shah Alam, Malaysia*
[d] *Atta-ur-Rahman Institute for Natural Products Discovery (AuRIns), Universiti Teknologi MARA (UiTM) Puncak Alam Campus, 42300 Puncak Alam, Selangor, Malaysia*
[e] *Department of Physics, Faculty of Science, Universiti Putra Malaysia, 43400 UPM Serdang, Selangor, Malaysia*
[f] *Industrial Technology Division, Malaysian Nuclear Agency, 43000 Kajang, Selangor, Malaysia*

This study investigates the eco-friendly synthesis of zinc oxide nanoparticles (ZnONPs) using Citrus hystrix extract as a reducing agent. HRTEM and SAED analyses confirmed spherical nanoparticles (~20 nm) with a hexagonal wurtzite structure. Photoluminescence (PL) results showed that lower zinc acetate concentrations (0.1 M) produced higher luminescence intensity, indicating an inverse relationship between concentration and optical properties. Antibacterial tests against five bacterial strains revealed greater efficacy at lower concentrations (0.1 M and 0.2 M), likely due to reduced aggregation. Raman spectroscopy confirmed the hexagonal wurtzite phase. Optimizing nanoparticle concentration could enhance applications in optoelectronics and catalysis. Lower concentrations (0.1 M and 0.2 M) often exhibited stronger antibacterial action against bacterial strains such S. aureus, E. coli, S. typhimurium, K. pneumoniae, and B. subtilis. The antibacterial performance of the ZnONPs was concentration-dependent. Lower doses produced the largest zones of inhibition; 0.2 M was the most effective against S. aureus, while 0.1 M was the most effective against S. typhimurium and B. subtilis.

1. Introduction

The synthesis and application of nanomaterials have become a growing field of research due to their unique physicochemical properties. Among these materials, zinc oxide nanoparticles (ZnONPs) have garnered significant attention for their wide range of applications, particularly in electronics, optoelectronics, and biomedicine. ZnO is a well-known semiconductor with a wide band gap (3.37 eV) and large exciton binding energy (60 meV) at room temperature, making it ideal for various optical and electronic devices. In recent years, ZnONPs have also demonstrated promising antimicrobial activity, which has opened new possibilities for their use in medical treatments, food packaging, and environmental protection. Several studies have proposed that aqueous suspensions of ZnO produce increased levels of reactive oxygen species (ROS), mostly hydroxyl radicals, H_2O_2

and singlet oxygen, which contribute to the antibacterial activity of ZnO nanoparticles [1] . The antibacterial properties of ZnONPs are mainly attributed to their ability to generate reactive oxygen species (ROS) and release zinc ions (Zn^{2+}), which disrupt bacterial cell membranes and other cellular components. Furthermore, green synthesis methods have emerged as eco-friendly alternatives to conventional chemical and physical synthesis approaches, offering a sustainable route for the production of ZnONPs with enhanced antibacterial efficacy.

The synthesis method plays a crucial role in determining the size, shape, surface properties, and antibacterial efficacy of ZnONPs. Conventional synthesis techniques, such as chemical precipitation, sol-gel methods, and hydrothermal approaches, often require high temperatures, toxic chemicals, and extensive energy consumption. In contrast, green synthesis methods utilizing plant extracts, microorganisms, or other biological agents provide a sustainable and eco-friendly alternative [2] . Plant-mediated synthesis, in particular, has gained popularity due to its simplicity, scalability, and use of natural reducing and stabilizing agents present in plant extracts. Extracts from plants may act both as reducing and capping agents in nanoparticle synthesis [2] . These green methods not only reduce the environmental impact of nanoparticle production but also produce ZnONPs with enhanced biocompatibility and reduced toxicity, making them more suitable for biomedical applications. For instance, Citrus hystrix extract, rich in bioactive compounds such as flavonoids and polyphenols, has been successfully used to synthesize ZnONPs with excellent antibacterial and optical properties.

Numerous studies have demonstrated that the antibacterial activity of ZnONPs is highly dependent on factors such as particle size, morphology, surface charge, and concentration. Smaller nanoparticles tend to exhibit higher antibacterial efficacy due to their larger surface area-to-volume ratio, which enhances their interaction with bacterial cells [3] . The surface charge of ZnONPs also plays a critical role in determining their antibacterial effectiveness, as positively charged nanoparticles are more likely to bind to negatively charged bacterial cell membranes. Additionally, the concentration of ZnONPs influences their aggregation behavior, bioavailability, and ability to penetrate bacterial cells. Lower concentrations are often more effective in preventing nanoparticle aggregation, thereby maintaining a higher surface area for interaction with bacterial cells. Studies have shown that optimizing ZnONP concentration can significantly improve their antibacterial performance, with lower concentrations yielding better results against specific bacterial strains such as *S. typhimurium* and *B. subtilis.*

For green synthesis, several plant parts are utilized, including the leaf, stalk, root, gum extract, flower, and fruit. These components are also employed to make the extract for the synthesis. It is reasoned that phytochemicals present in plant extracts act as an agent that helps reduce and stabilize ZnONPs and act as a capping and synthesizing agent [4]. Certain plants serve as sources of zinc ions for the green synthesis process, acting as zinc accumulators. The objective of this research is to employ an environmentally friendly method utilizing citrus hystrix extracts to synthesize multiple zinc oxide nanoparticles (ZnONPs).

2. Experimental details

Citrus hystrix, commonly known as kaffir lime, was selected for the green synthesis of zinc oxide nanoparticles (ZnONPs) due to its abundant availability and potential for bioreduction. The taxonomic classification of C. hystrix is presented in Table 1.

Table 1. Taxonomy of C. hystrix.

Family	Rutaceae
Sub-family	Aurantioideae
Genus	Citrus
Species	Citrus hystrix

The biosynthesis of ZnONPs was carried out using an extract derived from C. hystrix fruit. Initially, fresh fruits were thoroughly rinsed with deionized water and allowed to air dry at ambient temperature. After drying, the fruits were halved, and the juice was manually extracted. The obtained juice was filtered through muslin cloth to eliminate particulate matter. The clear extract was subsequently refrigerated at 4 ºC for use in further experiments.

For nanoparticle synthesis, 50 mL of deionized water was mixed with 0.1 M zinc acetate dihydrate, and the mixture was stirred continuously for one hour using a magnetic stirrer. Once the stirring phase was complete, 25 mL of C. hystrix extract was added to the solution, followed by titration with NaOH to adjust the pH to 12. The reaction mixture was stirred rigorously at 500 rpm for an additional three hours. A visible color shift from milky yellow to brownish yellow indicated the successful formation of ZnO nanoparticles.
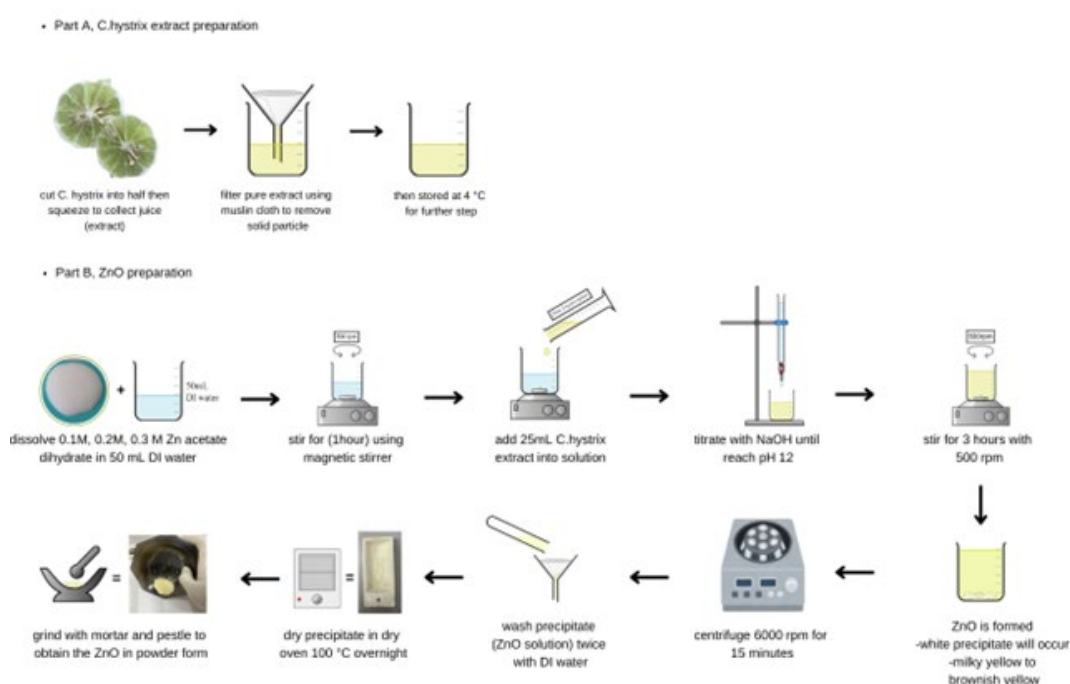

Fig. 1. Synthesis process of zinc oxide (ZnO)

Table 2. Parameter used in the experiment.

Parameter	Value
Concentration of NaOH	0.1 M
Concentration of Zinc Acetate	1.0 M, 2.0 M and 3.0 M
Volume of Citrus Hystrix extracts	25 mL
pH level reached (fixed)	pH 12

The antibacterial test will be performed according to the disc diffusion method using Muller Hint on agar. In this work, bacterial strains of Escherichia coli and Staphylococcus aureus will be employed during the anti-bacterial test. The above-mentioned bacteria will be grown individually on Whatman no.1 filter discs at 37℃ for 24 hours. ZnONPs calcined with different temperatures will exhibit remarkable antibacterial activity against all tested bacterial strains. Using a sterile cotton swab the test organisms will be swabbed over the surface of the agar plates. Then it is incubated in

the presence of antimicrobial materials. If the bacterial or fungal strain is susceptible to the antimicrobial agent, then a zone of inhibition will appear on the agar plate. If it resists the antimicrobial agent, then it can be concluded that no zone is evident. After that, the zone of inhibition will be observed using the microscope.

3. Results and discussion

In order to strengthen the evidence supporting the synthesis of biogenic ZnONPs, HRTEM was carried out. Sample size, shape, and internal structure can be examined using High-Resolution Transmission Electron Microscopy (HRTEM) equipment. The HRTEM images reveal that the ZnO nanoparticles are predominantly spherical with an average size of around 20 nm. The lattice fringes and Selected Area Electron Diffraction (SAED) patterns confirm that the particles have a high degree of crystallinity with a hexagonal wurtzite structure. The d-spacing values obtained from the lattice fringes match well with the known values for ZnO, further verifying the material's composition and crystalline phase.

As seen in Figure 2, the HRTEM micrograph demonstrates the morphology of the biogenic ZnONPs, which have a spherical-like shape with tiny particles of varying sizes and aggregated with a size range of 50 to 20 nm. The aggregation of nanoparticles occurred due to the large surface area to volume ratio of the biogenic ZnONPs [5]. Using High-Resolution Transmission Electron Microscopy (HRTEM), the ZnO nanoparticles were found to be spherical with an average size of around 20 nm. The images also showed clear, repeating patterns called lattice fringes, confirming the particles are highly crystalline. Additionally, the analysis confirmed that the nanoparticles have a hexagonal structure, which is typical for ZnO. This means the synthesis process successfully created well-defined, crystalline ZnO nanoparticles, suitable for applications in fields like electronics and catalysis.
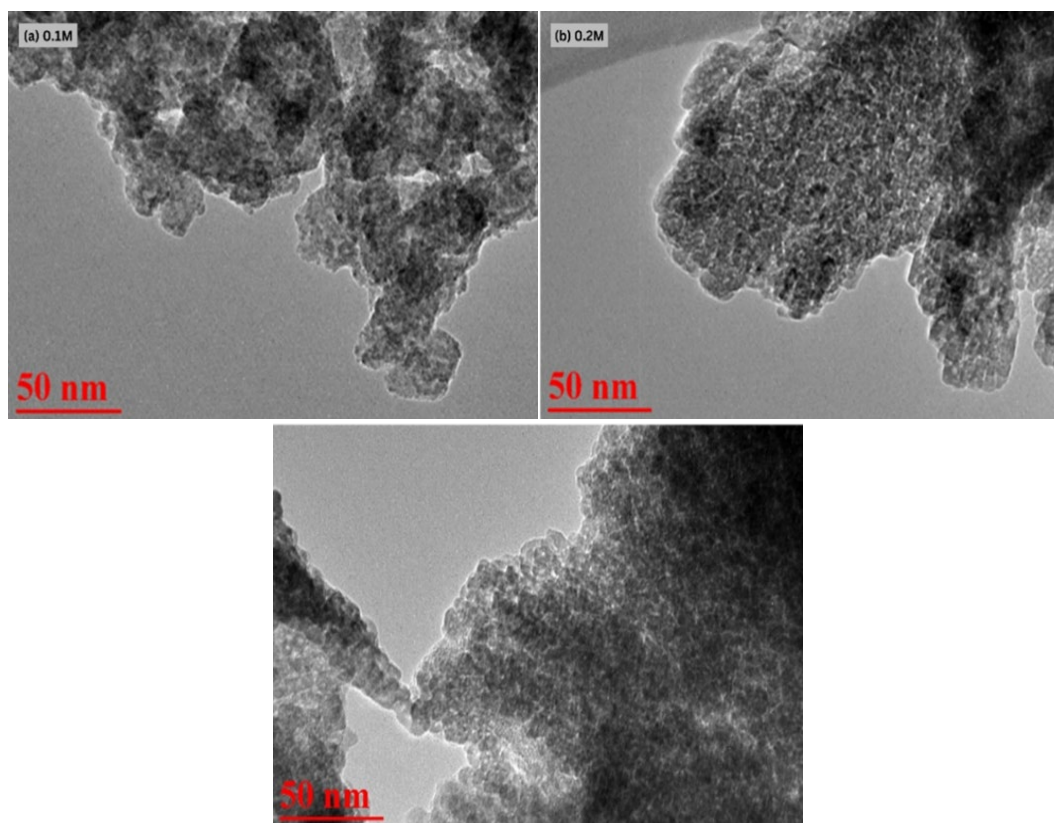

Fig. 2. HRTEM micrographs of biogenic ZnONPs synthesized at different concentrations on 100,000X magnification.

To investigate the optical properties of biogenic ZnONPs, Photoluminescence (PL) studies was employed. The nanoparticles were subjected to an excitation wavelength of 400 nm, and the resulting emission spectra were recorded. The PL measurements were conducted under controlled conditions to ensure accurate and reliable results. The ZnONPs exhibited emission peaks at 486 nm, 259 nm, and 126 nm when synthesized at concentrations of 0.1 M, 0.2 M, and 0.3 M, respectively as shown in Figure 3. These findings suggest a relationship between ZnONP concentration and their emission properties. While the excitation and emission spectra of ZnONPs remained consistent across different zinc acetate concentrations, their luminescence intensities demonstrated a clear inverse relationship, with lower concentrations yielding higher luminescence. The observed emission spectra were exclusively within the blue region of the visible spectrum, with a maximum intensity at 486 nm which attributed to the radioactive recombination of a photogenerated hole with an electron occupying the oxygen vacancy [6].
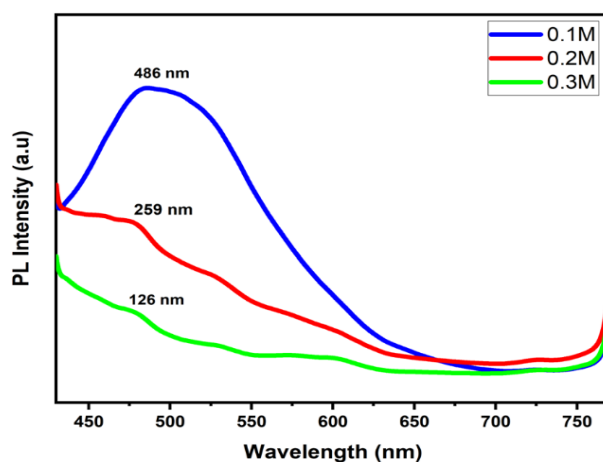

Fig. 3. The PL spectrum for biogenic ZnONPs synthesized at different concentrations.

Raman spectroscopy has proven important in material science for examining nanomaterials, including metal oxides, carbon-based materials, and biological samples. It makes it possible to determine the lattice structure's crystalline phases, defects, and stress strain. Figure 4 displays the Raman spectrum recorded for biosynthesized ZnO nanoparticles in the spectral range of 100-1000 cm^{-1}. The crystal structure of ZnO is wurtzite (hexagonal) which belongs to the C_{6V}^4 space group having two formula units per primitive cell with all the atoms occupying the C_{3v} sites [7]. According to Group theory, the zone-center optical phonon modes of ZnO are predicted to consist of eight distinct sets. Among these, the A_1 and E_1 modes are polar, resulting in a splitting into transverse optical (TO) and longitudinal optical (LO) phonons. The E_2 mode, on the other hand, is composed of two Raman-active phonons, a low-frequency E_2L mode and a high-frequency E_2H mode [8]. Considering the transverse-optical (TO) and longitudinal-optical (LO) phonons in A_1 and E_1 are polar phonons, each of them has different frequencies.

The Raman spectrum presented in Figure 4 depicts the scattering profiles of ZnO nanoparticles synthesized at three different precursor concentrations 0.1 M, 0.2 M, and 0.3 M. The distinct peaks correspond to characteristic vibrational modes of ZnO, and their intensities vary with concentration, indicating changes in crystallinity and structural properties. The prominent peak at around 9498 cm^{-1} observed for all concentrations signifies a strong phonon mode, potentially the E_2 (high) mode, which is characteristic of the hexagonal wurtzite phase of ZnO. The presence of multiple peaks at lower wavenumbers, such as at 349 cm^{-1}, 1132 cm^{-1}, and 1381 cm^{-1}, suggests variations in lattice vibrations, likely due to differences in particle size and surface defects across the samples.
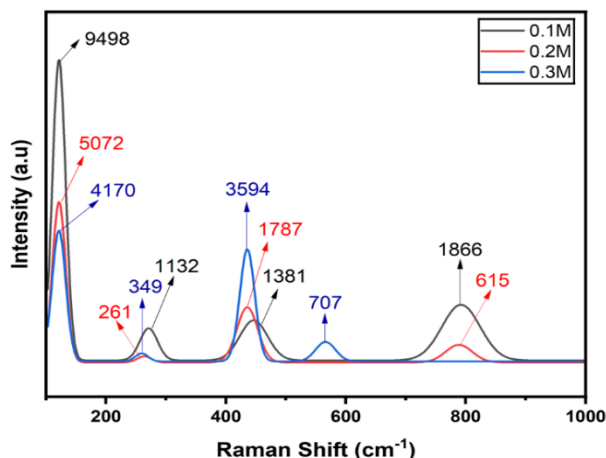
Fig. 4. Raman spectra of ZnO nanoparticles synthesized at varying precursor concentrations.

In addition, the shifts in peak intensities across the different concentrations, such as the significant increase at 4170 cm^{-1} and 3594 cm^{-1} with increasing concentration, indicate that the structural characteristics of the ZnO nanoparticles are influenced by the precursor molarity. The peaks at 1866 cm^{-1} and 615 cm^{-1}, which show variation in intensity with increasing concentration, may be attributed to defect-related modes, such as oxygen vacancies or zinc interstitials. These findings highlight the concentration-dependent structural properties of the ZnO nanoparticles, with higher precursor concentrations likely contributing to improved crystallinity and defect states, which are clearly reflected in the Raman spectral features.

Figure 5 illustrates the zones of inhibition produced by 0.1M, 0.2M and 0.3M biogenic ZnONP and a positive control in five different types of bacteria. The clear zones observed in Figure 5 indicate the inhibition of bacterial growth by biogenic ZnONPs sample. Table 3 presents the results of testing the inhibition zone of biogenic ZnONPs generated at varying doses on antibacterial activity against *S. aureus, E. coli, S. typhimurium, K. pneumoniae and B. subtilis* using the disk diffusion method.
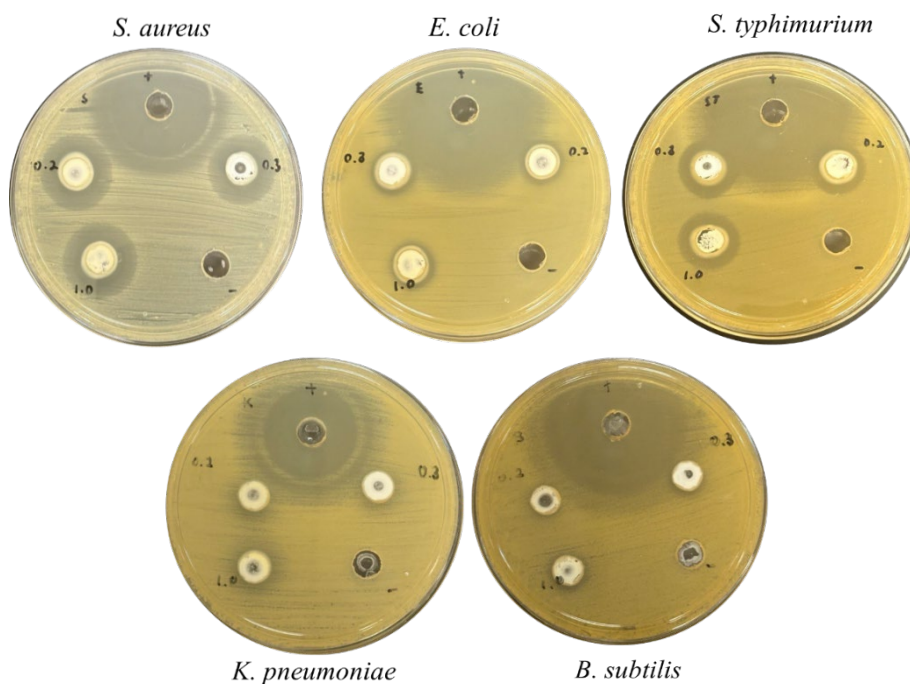

Fig. 5. Inhibition zone of synthesized biogenic ZnONPs in different types of bacteria.

The graph shown in Figure 6 represents the data from the Table 3, comparing the diameter of inhibition zones for different bacterial strains in response to ciprofloxacin (positive control) and the sample at three concentrations (0.1 M, 0.2 M, 0.3 M). The antibacterial activity of the sample was evaluated at three concentrations (0.1 M, 0.2 M, and 0.3 M) across five bacterial strains. The results indicate that the effectiveness did not increase consistently with higher concentrations. For S. aureus, the inhibition zone was largest at 0.2 M (21.33 mm), slightly higher than at 0.1 M (20.67 mm). Similarly, E. coli showed its highest inhibition at 0.2 M (15.33 mm), compared to 14.67 mm at 0.1 M. However, for S. typhimurium and B. subtilis, the largest zones were observed at 0.1 M, with inhibition zones of 21.0 mm and 20.67 mm, respectively, both of which decreased as the concentration increased. For K. pneumoniae, the inhibition zone peaked at 0.2 M (14.67 mm) but was relatively small across all concentrations.

Overall, the data suggest a non-linear relationship between sample concentration and antibacterial activity, as higher concentrations (0.3 M) generally resulted in diminished effectiveness. For instance, S. aureus exhibited a reduced inhibition zone of 19.33 mm at 0.3 M, and E. coli dropped to 12.33 mm. This trend was also seen in S. typhimurium and B. subtilis, which showed reduced activity at higher concentrations. Thus, the 0.1 M concentration was most effective for S. typhimurium and B. subtilis, while 0.2 M was optimal for S. aureus and E. coli. Increasing the concentration to 0.3 M generally led to reduced antibacterial efficacy.

In conclusion, the antibacterial activity of the sample varied depending on the concentration and bacterial strain, with no consistent improvement at higher concentrations. The impact of biogenic ZnONPs' nanoparticle size is another aspect that could prevent the concentration increase from affecting the inhibition of bacteria. The bacterial cells get dislocated and disrupted due to the permeability of the sample entering the bacterial membrane, which is caused by the nanoparticle size of biogenic ZnONPs hence the inhibition of bacteria growth occurred [9]. When biogenic ZnONPs come into direct contact with bacterial cells, they also release Zn2+ ions, which kills the cell. The toxic effect of biogenic ZnONPs produces from the ROS also cause the bacterial death cell [10]. Recently, the ZnONPs were successfully to prevent the progression of carbapenems-resistant by generating ROS and producing membrane damage [11]. The existence of super oxide anion and hydrogen peroxide in the cells were the results of ZnONPs [12, 13, 14]. The lipid peroxidation processs believed to produce the membrane leakage of proteins and nucleic acids in the cell membranes [14].

Table 3. Antibacterial test of biogenic ZnONPs synthesized at 0.1M, 0.2M, 0.3M and ciprofloxacin (positive control).

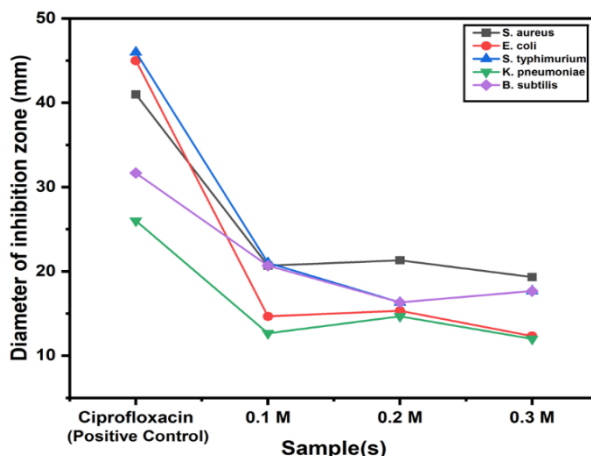|	Samples	Diameter of inhibition zone (mean±s.d) (mm)				
		Bacteria				
		S. aureus	E. coli	S. typhimurium	K. pneumoniae	B. subtilis
1	Ciprofloxacin (Positive Control)	41.0±0.82	45.0±5.0	46.0±1.73	26.0±1.0	31.67±0.47
2	0.1 M (100 mg/ml)	20.67±0.94	14.67±0.47	21.0±0.94	12.67±0.47	20.67±0.94
3	0.2 M (100 mg/ml)	21.33±0.94	15.33±0.47	16.33±0.47	14.67±0.94	16.33±0.47
4	0.3 M (92 mg/ml)	19.33±0.47	12.33±0.47	17.67±0.47	12.0±1.0	17.67±0.46

Fig. 6. The diameter of inhibition zone of biogenic ZnONPs prepared at different concentrations.

4. Conclusion

The present study successfully demonstrated the green synthesis of zinc oxide nanoparticles (ZnONPs) using Citrus hystrix extract, showcasing a sustainable and eco-friendly approach. Characterization techniques, including High-Resolution Transmission Electron Microscopy (HRTEM) and Selected Area Electron Diffraction (SAED), confirmed that the biogenic ZnONPs possessed a predominantly spherical shape with an average size of approximately 20 nm and a hexagonal wurtzite structure. The high crystallinity, verified by clear lattice fringes and matching d-spacing values, demonstrated that the green synthesis method retained the integrity of the ZnO crystalline phase. Photoluminescence (PL) spectroscopy revealed concentration-dependent luminescence properties, with the highest emission intensity at the lowest zinc acetate concentration (0.1 M). The blue-shifted emission peaks across all concentrations indicated the high optical quality of the nanoparticles, suggesting minimal defect states. This inverse relationship between ZnONP concentration and luminescence intensity suggests that optimizing nanoparticle concentration could enhance optical properties, making these biogenic ZnONPs promising for optoelectronic and photonic applications.

The antibacterial efficacy of the ZnONPs was concentration-dependent, with lower concentrations (0.1 M and 0.2 M) generally showing greater antibacterial activity against bacterial strains such as S. aureus, E. coli, S. typhimurium, K. pneumoniae, and B. subtilis. The highest zones of inhibition were observed at lower concentrations, with the 0.2 M concentration being most effective against S. aureus and 0.1 M performing best against S. typhimurium and B. subtilis. This behavior is likely due to nanoparticle aggregation at higher concentrations, reducing surface area and bioavailability. Raman spectroscopy confirmed the high crystallinity of the ZnONPs, with peaks corresponding to the hexagonal wurtzite phase, and variations in peak intensities reflecting concentration-dependent defect states. These results underscore the importance of precursor concentration in influencing both the optical and antibacterial properties of ZnONPs. Overall, the study highlights the potential of biogenic ZnONPs for diverse applications, including antibacterial treatments, electronics, and catalysis, and emphasizes the need to optimize nanoparticle concentration for specific uses.

References

[1] Raghupathi, K. R., Koodali, R. T., Manna, A. C. (2011), Langmuir, 27(7), 4020–4028; https://doi.org/10.1021/la104825u

[2] Iravani, S. (2011), Green Chemistry, 13(10), 2638–2650; https://doi.org/10.1039/c1gc15386b

[3] Silva, B. L. da, Abuçafy, M. P., Manaia, E. B., Junior, J. A. O., Chiari-Andréo, B. G., Pietro, R. C. L. R., Chiavacci, L. A. (2019), International Journal of Nanomedicine (Vol. 14, pp. 9395–9410). Dove Medical Press Ltd; https://doi.org/10.2147/IJN.S216204

[4] Rai, R. S., P, G. J., Bajpai, V., Khan, M. I., Elboughdiri, N., Shanableh, A., Luque, R. (2023), Environmental Research, 221; https://doi.org/10.1016/j.envres.2022.114807

[5] W. G. Anbuvannan, M., Ramesh, M., Viruthagiri, G., Shanmugam, N., Kannadasan, N. (2015), Spectrochimica Acta - Part A: Molecular and Biomolecular Spectroscopy, 143, 304–308; https://doi.org/10.1016/j.saa.2015.01.124

[6] Sangeetha, G., Rajeshwari, S., Venckatesh, R. (2011), Materials Research Bulletin, 46(12), 2560–2566; https://doi.org/10.1016/J.MATERRESBULL.2011.07.046

[7] Khan, A. (2010), J Pak Mater Soc (Vol. 4, Issue 1).

[8] Khan, A., Kordesch, M. E. (2007), Materials Letters, 62(2), 230–234; https://doi.org/10.1016/j.matlet.2007.05.005

[9] Bhuyan, T., Mishra, K., Khanuja, M., Prasad, R., Varma, A. (2015), Materials Science in Semiconductor Processing, 32, 55–61; https://doi.org/10.1016/j.mssp.2014.12.053

[10] Lingaraju, K., Raja Naika, H., Manjunath, K., Basavaraj, R. B., Nagabhushana, H., Nagaraju, G., & Suresh, D. (2016), Applied Nanoscience (Switzerland), 6(5), 703–710; https://doi.org/10.1007/s13204-015-0487-6

[11] Tiwari, V., Mishra, N., Gadani, K., Solanki, P. S., Shah, N. A., Tiwari, M. (2018), Frontiers in microbiology, 9, 1218; https://doi.org/10.3389/fmicb.2018.01218

[12] Kumar, A., Pandey, A. K., Singh, S. S., Shanker, R., Dhawan, A. (2011), Free Radical Biology and Medicine, 51(10), 1872-1881; https://doi.org/10.1016/j.freeradbiomed.2011.08.025

[13] Horie, M., Fujita, K., Kato, H., Endoh, S., Nishio, K., Komaba, L. K., Iwahashi, H. (2012), Metallomics, 4(4), 350-360; https://doi.org/10.1039/c2mt20016c

[14] Singh, P., Garg, A., Pandit, S., Mokkapati, V. R. S. S., Mijakovic, I. (2018), Nanomaterials, 8(12), 1009; https://doi.org/10.3390/nano8121009